Structural Chemistry (2019) 30:2327–2338
https://doi.org/10.1007/s11224-019-01428-4

ORIGINAL RESEARCH

Cytotoxicity of doxorubicin conjugated with C_{60} fullerene. Structural and in vitro studies

Kamila Butowska[1,2] · Witold Kozak[2] · Magdalena Zdrowowicz[2] · Samanta Makurat[2] · Michał Rychłowski[3] · Aleksandra Hać[4] · Anna Herman-Antosiewicz[4] · Jacek Piosik[1] · Janusz Rak[2]

Received: 8 May 2019 / Accepted: 20 September 2019 / Published online: 22 October 2019

Abstract

Conjugating an anticancer drug of high biological efficacy but large cytotoxicity with a "transporting" molecule of low toxicity constitutes a valuable approach to design safe drug delivery system. In the present study, doxorubicin (DOX) a drug of large cardiotoxicity was chemically conjugated to a C_{60}-fullerene. The synthesized molecule, a fullerene-doxorubicin conjugate (Ful-DOX), was characterized using the ^{1}H NMR and MALDI TOF mass spectrometry. The absorption and fluorescence spectra and dynamic light scattering of the conjugate were recorded in an aqueous solution, while the impact on viability of several cancer cell lines of the free DOX and the conjugate was compared using the SRB and WST-1 assays. A low antiproliferative activity of the conjugate as compared to the free DOX is a consequence of the presence of fullerene moiety in the former, which is also responsible for the conjugate aggregation in an aqueous solution. Unlike free DOX, these aggregates cannot pass through the nuclear membrane (as demonstrated by the confocal microscopy measurements), which makes them marginally cytotoxic.

Keywords Fullerene · Doxorubicin · Covalent conjugate · Drug delivery · Nanoparticle · Cancer cells

Introduction

Doxorubicin (DOX; for its chemical structure, see Fig. 1) is well known for its anticancer activity. Furthermore, it is commonly used in clinics against various types of cancer in adults and children [1, 2]. Many studies have attributed DOX anticancer activity to intercalation into tumor cellular DNA, DNA cross-linking, binding to proteins involved in DNA replication and transcription, like topoisomerase II, as well as to generation of reactive oxygen species [3, 4]. Unfortunately, DOX cannot be applied at optimal doses mainly due to its cardiotoxic effects [5]. Although doxorubicin affects the brain, kidney, and liver, the heart seems to be the preferential target for its toxicity [6]. Actually, acute cardiotoxicity is observed in about 11% of patients exposed to DOX [7, 8], while the incidences of chronic myopathy are much less common and estimated to occur in ca 1.7% of cases [9].

Despite the fact that DOX-induced cardiotoxicity has been observed and studied for many years, the mechanism lying behind the toxic effect is still unclear [2]. Several models of cardiotoxicity have been proposed so far. Topoisomerase II, which is suppressed by DOX, was identified as a cardiotoxicity mediator [10]. On the other hand, oxidative stress, mediated by doxorubicin via enzymatic route employing intracellular or intramitochondrial oxidant enzymes, produces hydroxyl radicals that trigger DNA damage, protein modification, lipid peroxidation, and finally cell death by apoptosis or necrosis, which is considered as the main reason for DOX cardiotoxicity [2]. In the context of

Electronic supplementary material The online version of this article (https://doi.org/10.1007/s11224-019-01428-4) contains supplementary material, which is available to authorized users.

✉ Janusz Rak
janusz.rak@ug.edu.pl

Jacek Piosik
jacek.piosik@biotech.ug.edu.pl

[1] Laboratory of Biophysics, Intercollegiate Faculty of Biotechnology of the University of Gdańsk and Medical University of Gdańsk, Abrahama 58, Gdańsk, 80-307, Poland

[2] Laboratory of Biological Sensitizers, Faculty of Chemistry, University of Gdańsk, Wita Stwosza 63, Gdańsk, 80-308, Poland

[3] Department of Virus Molecular Biology, Intercollegiate Faculty of Biotechnology of the University of Gdańsk and Medical University of Gdańsk, Abrahama 58, Gdańsk, 80-307, Poland

[4] Department of Medical Biology and Genetics, Faculty of Biology, University of Gdańsk, Wita Stwosza 59, Gdańsk, 80-308, Poland

cardiotoxicity, the literature mentions also that DOX impaired Ca^{2+} handling [11], activated p53-dependent pathways [12], and cytochrome c mediated apoptosis via activation of caspase 9 and 3 [13].

As indicated above, the DOX-induced cardiotoxicity is coupled to an interaction between the anthracycline and a number of proteins. Therefore, a promising way of alleviating its toxic effects seems to be DOX binding into a sufficiently large molecule that would impair the protein-DOX interactions necessary to trigger the DOX toxicity. After accumulation in cancer cells, such a conjugate should release DOX, which only then could cause the lethal effects.

Fullerenes seem to be suitable drug carriers due to the stability of their cage and a relative ease to functionalization [14]. The literature shows that there were already several attempts to employ fullerenes as drug carries [15]. Both van der Waals (vdW) complexes between the delivered drugs and a fullerene as well as fullerene-drug covalent conjugates were considered for this purpose. For instance, fullerene-DOX complexes, in which the release of DOX was pH-dependent, were prepared and characterized with capillary electrophoresis [16]. Similarly, a complex of fullerene-based carrier with cisplatin (well-known anticancer agents) was tested against lung cancer [17]. Eventually, the enhancement, as compared to the free drugs, of anticancer activity of DOX and cisplatin vdW complexes with a C_{60}-fullerene derivative, has been reported recently [18]. On the other hand, a C_{60}-fullerene-paclitaxel covalent conjugate was proposed as a slow release drug-delivery system [19]. Furthermore, a molecular system in which DOX is conjugated to the C_{60} fullerene via a reactive thioketal linker sensitive to the reactive oxygen species (ROS) was tested on a mouse model [20]. The conjugate, of excellent stability in physiological environment, releases DOX due to the photoinduced generated ROS by the excited C_{60}-fullerene that in turn leads to the breakage of the linker. A conjugate strategy was also tested on poly(ethylene glycol) (PEG) connected to DOX and fullerene [21, 22].

Surprisingly, DOX coupled to C_{60} through a PEG spacer showed similar cytotoxicity against the MCF-7 cells as the free DOX [20]. The observed effect was explained by different mode of action related to the free DOX and fullerene-DOX conjugate. The latter was claimed to be capable of inducing toxic effects in the cytoplasm; thus, in the light of ref. [21], the accumulation of DOX in nucleus might not be a prerequisite of the drug activity. These unexpected and anti-intuitive results prompted us to investigate the cytotoxicity of a similar fullerene-DOX conjugate. In the following, we describe a five-step chemical synthesis of a C_{60}-DOX conjugate coupled by a PEG linker. Using ^{1}H NMR spectroscopy and high-resolution MALDI-TOF mass spectrometry, we prove the identity of all intermediate products and the final conjugate. The structure of obtained conjugate is characterized physicochemically with the help of several techniques like absorption and emission spectroscopy as well as dynamic light scattering. Furthermore, the toxicity of the obtained material is tested using two viability assays: SRB and WST-1. Finally, the distribution of the conjugate or the drug in the MCF-7 cells after 2-day incubation with the conjugate or DOX is shown by confocal microscopy. Our investigations unequivocally indicate that DOX covalently conjugated to C_{60}-fullerene is nontoxic in concentrations in which the free drug reduces cell viability by ca 50%.

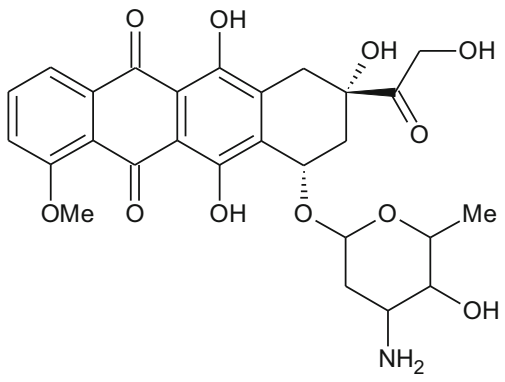

Fig. 1 Chemical structure of DOX

Experimental and computational

Chemicals and reagents

t-Butyl 12-hydroxy-4,7,10-trioxadodecanoate, carbon tetrabromide, 1,8-diazabicyclo[5.4.0]undec-7-ene (DBU), dicyclohexylcarbodiimide (DCC), doxorubicin hydrochloride, fullerene-C_{60}, malonyl chloride, *N*-hydroxysuccinimide (NHS), trifluoroacetic acid (TFA), trimethylamine (TEA), and dimethyl sulfoxide (DMSO) were purchased from Sigma-Aldrich. Dichloromethane (DCM) was dried and distilled using standard procedures. Anhydrous *N*,*N*-dimethylformamide (DMF) and toluene were both available from Sigma-Aldrich. Column chromatography was performed using silica gel NORMASIL 60 (40–63 mesh, VWR Chemicals). Thin-layer chromatography was performed with silica gel plates, 60G, F254 (Sigma-Aldrich). RPMI cell culture medium, penicillin/streptomycin antibiotic mixture, and fetal bovine serum were purchased from Corning, while F12 medium in Kaingh modification (F12K) from Gibco. Hoechst 33342 was purchased from ThermoFisher Scientific.

Synthesis of bis(14,14-dimethyl-12-oxo-3,6,9,13-tetraoxapentadecyl) malonate 3 (for the structure see Scheme 1)

Malonyl chloride **1** (0.22 mL, 2.29 mmol) was added to the solution of *t*-butyl 12-hydroxy-4,7,10-trioxadodecanoate **2**

(1.34 g, 4.81 mmol) in dry DCM (10 mL). The mixture was cooled to 0 °C and TEA (0.80 mL, 5.73 mmol) was added. The solution was allowed to warm to room temperature and stirred for 72 h. The reaction was quenched with water (5 mL). The organic layer was separated and the remaining water phase was extracted with DCM (3 × 15 mL). Combined organic layers were dried over $MgSO_4$ and evaporated. The resulting residue was purified by column chromatography using DCM/MeOH 30/1 as an eluent to give the desired product as a yellowish oil in a 58% yield.

^{1}H NMR (Bruker AVANCE III, 500 MHz, $CDCl_3$), δ: 1.47 (s, 18H, CH_3), 2.52 (t, 4H, $J = 6.6$, CH_2), 3.47 (s, 2H) 3.62–3.69 (m, 16H, CH_2), 3.73 (t, 8H, $J = 5.6$, CH_2), 4.32 (t, 4H, $J = 4.7$, CH_2); HRMS (AB SCIEX MALDI TOF/TOF 5800), m/z: $[M-H]^-$ calcd for $C_{29}H_{51}O_{14}$ 623.7140, found 623.2510 (see Figs. S1 and S2, Supplementary Information).

Synthesis of bis(14,14-dimethyl-12-oxo-3,6,9,13-tetraoxapentadecyl) C_{60}–malonate 4 (for the structure see Scheme 1)

To a solution of C_{60}-fullerene (50 mg, 0.069 mmol) in dry toluene (20 mL), malonic ester derivative **3** (37 mg, 0.059 mmol), CBr_4 (20 mg, 0.059 mmol), and DBU (10 μL, 0.066 mmol) were added. The mixture was stirred overnight at room temperature. After that, toluene was evaporated and the crude product was purified by column chromatography using toluene, to remove the unreacted fullerene-C_{60}, and then DCM/MeOH 50/1 as an eluent to give the desired product as a brown solid in a 63% yield.

HRMS (AB SCIEX MALDI TOF/TOF 5800), m/z: $[M-H]^-$ calcd for $C_{89}H_{49}O_{14}$ 1342.3412, found 1342.1563 (see Fig. S3, Supplementary Information).

Synthesis of 15-C_{60}-14,16-dioxo-4,7,10,13,17,20,23,26-octaoxanonacosane-1,29-dioic acid 5 (for the structure see Scheme 1)

The derivative **4** (50 mg, 0.037 mmol) was dissolved in DCM (15 mL) and TFA (15 mL) was added. The reaction was monitored by TLC analysis, and after the complete disappearance of the product (about 30 min), the mixture was evaporated and the crude product was purified by column chromatography using DCM/MeOH 30/1 as an eluent to give the desired compound as a brown solid in a quantitative yield.

HRMS (AB SCIEX MALDI TOF/TOF 5800), m/z: $[M-H]^-$ calcd for $C_{81}H_{33}O_{14}$ 1230.1286, found 1230.1058 (Fig. S4, Supplementary Information).

Synthesis of bis(2-(2-(2-(3-((2,5-dioxopyrrolidin-1-yl)oxy)-3-oxopropoxy)ethoxy)ethoxy)ethyl) C_{60}–malonate 6 (for the structure see Scheme 1)

To a solution of the derivative **5** (50 mg, 0.041 mmol) in DCM (20 mL), NHS (21 mg, 0.180 mmol) and a solution of DCC (21 mg, 0.102 mmol) in DCM (5 mL) were added. The reaction mixture was left overnight. Then, the solvent was evaporated

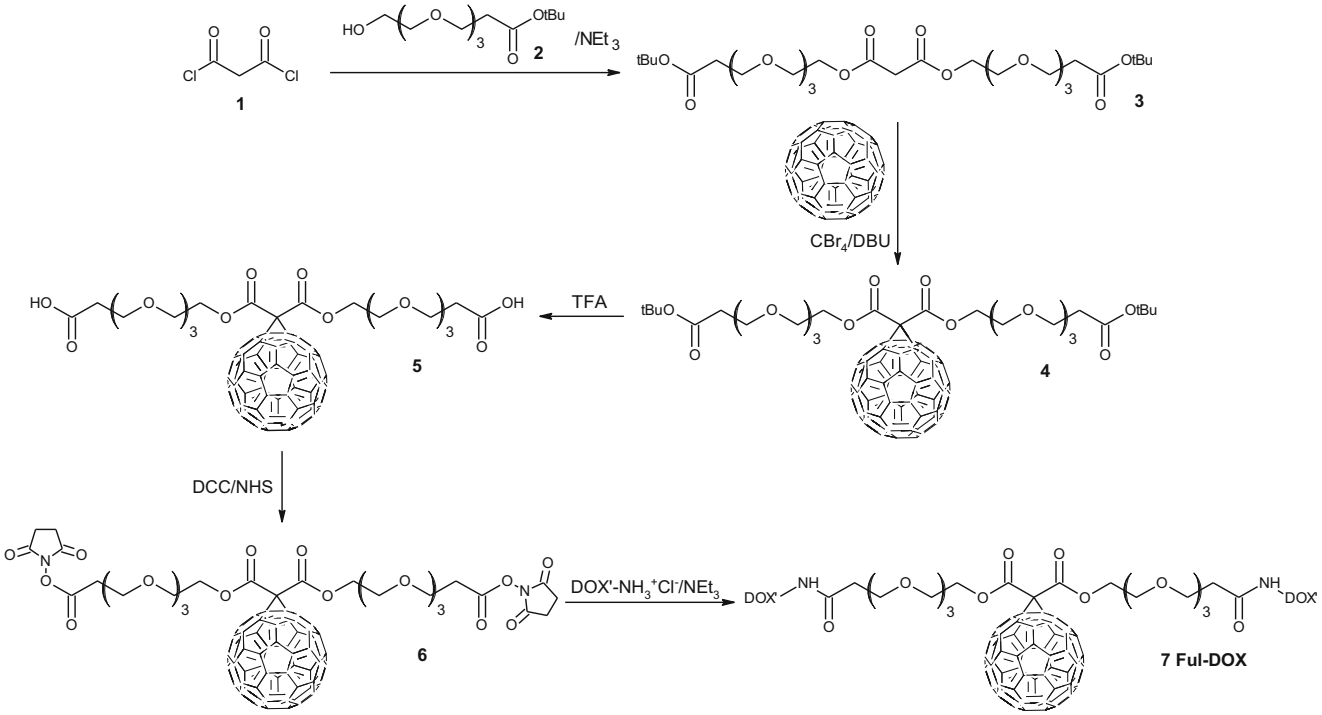

Scheme 1 Reaction route for the synthesis of Ful-DOX conjugate **7**

and the crude product was purified by column chromatography using DCM/MeOH 30/1. At this point, we eventually got a mixture of the desired product and DCU – a byproduct from the reaction of activation of carboxylic groups in **5**.

HRMS (AB SCIEX MALDI TOF/TOF 5800), m/z: $[M + Na]^+$ calcd for $C_{89}H_{40}N_2NaO_{18}$ 1448.2633, found 1447.1733 (see Fig. S5, Supplementary Information).

Synthesis of bis-doxorubicinyl amide of 15-C_{60}-14,16-dioxo-4,7,10,13,17,20,23,26-octaoxanonacosane-1,29-dioic acid 7 (Ful-DOX 7) (for the structure see Scheme 1)

The raw product **6** (50 mg, 0.035 mmol) was dissolved in dry DMF (2 mL). In the other flask, a solution of doxorubicin hydrochloride (41 mg, 0.070 mmol) in DMF (16 mL) was prepared. To the second mixture, TEA (10 μL, 0.070 mmol) was added. After 2–3 min, the DOX solution was added dropwise to the DMF solution of **6**. After 48 h of stirring at room temperature, the reaction mixture was evaporated azeotropically with toluene. The final product was purified by column chromatography using as an eluent, at first DCM/MeOH 30/1 (to remove DCU from the activation procedure) and then DCM/MeOH 20/1.

HRMS (AB SCIEX MALDI TOF/TOF 5800), m/z: $[M - H]^-$ calcd for $C_{135}H_{87}N_2O_{34}$ 2281.1365, found 2280.7888 (see Fig. S6, Supplementary Information).

NMR and MS analyses

The NMR spectrum was recorded on a Bruker AVANCE III, 500 MHz spectrometer. Chemical shifts are reported in ppm relative to the residual solvent peak ($CDCl_3$ = 7.28 ppm for ^1H). Coupling constants are given in Hertz. The MS measurements of the intermediates and final product were done with use of MALDI TOF/TOF 5800 (ABSciex, Germany). As a matrix, 2,5-dihydroxybenzoic acid (DHB, Sigma-Aldrich) was used. The measurements were done in reflectron negative ion mode with previous mass calibration with commercial standard (Sciex) for bis(14,14-dimethyl-12-oxo-3,6,9,13-tetraoxapentadecyl) malonate **3**, (14,14-dimethyl-12-oxo-3,6,9,13-tetraoxapentadecyl) C_{60}–malonate **4**, 15-C_{60}-14,16-dioxo-4,7,10,13,17,20,23,26-octaoxanonacosane-1,29-dioic acid **5** and bis-doxorubicinyl amide of the 15-C_{60}-14,16-dioxo-4,7,10,13,17,20,23,26-octaoxanonacosane-1,29-dioic acid **7**. For bis(2-(2-(2-(3-((2,5-dioxopyrrolidin-1-yl)oxy)-3-oxopropoxy)ethoxy)ethoxy)ethyl) C_{60}–malonate **6**, the measurement was done in reflectron positive ion mode. Samples were prepared using the dried droplet preparation method by mixing 0.6 mL of an analyte solution with 0.6 mL of matrix solution (directly on a plate). After air drying, the plate was introduced directly to the instrument. MS spectra were acquired from 499 to 2509 m/z for a total of 1000 laser shots by a 1-kHz OptiBeam laser (ND-YAG). Laser intensity remained fixed for all the analyses. Registered spectra were analyzed with Data Explorer software.

Theoretical calculations

The molecular structures of DOX, Fullerene C_{60}, and Ful-DOX conjugate 7 (see Fig. 2) were optimized at the PM6-D3 [23, 24] level of theory. Next, for geometries obtained at the PM6-D3 level, the UV–Vis spectra were calculated using the TD-DFT/B3LYP-D3 [25] method with the Def2SVP [26, 27] basis set and the PCM [28, 29] model to account for water solvation. This combination of functional and basis set was successfully applied before for the prediction of UV–Vis spectra of fullerene conjugates [30]. For fullerene and DOX, 50 states were computed, while for the larger structure of Ful-DOX, we calculated 150 states. All calculations were performed using the Gaussian09 suite [31].

Spectrophotometric measurements

Visible absorption spectra were measured on SPECORD 50 PLUS spectrophotometer (Analytik Jena AG, Jena, Germany) with stabilized temperature (25 ± 0.1 °C) in the wavelength range of 350–700 nm with 0.5 nm intervals. Spectra were measured in a quartz cuvettes (1 cm light path) containing 2 mL of 0.2 M sodium phosphate buffer, pH 6.8, and an aqueous DMSO (DMSO concentration up to 10%) solution containing 0.036 mM DOX, 0.029 mM Ful-DOX conjugate **7,** and 0.029 mM C_{60}-fullerene.

Spectrofluorimetric measurements

All fluorescence measurements were carried out on a Jasco FP-8500 Spectrofluorometer equipped with a 150 W xenon lamp with stabilized temperature (25 ± 0.1 °C), using 1 cm quartz cuvettes in the wavelength range of 500–750 nm with 0.5 nm intervals. Experiments were done in 2 mL of 0.2 M sodium phosphate buffer, pH = 6.8. The Ful-DOX conjugate **7** fluorescence spectrum (excitation wavelength = 476 nm and emission wavelength = 548–650 nm) was measured (concentration range: 0.003–0.163 mM) and maximum fluorescence peak was observed at 593 nm. The obtained data are expressed in the mean relative fluorescence units (RFU).

Dynamic light scattering (DLS) characterization

DLS analysis was performed on Zetasizer Nano ZS (Malvern, Worcestershire, UK) by measuring the intensity of the scattered light for aqueous DMSO solution of 0.015 mM Ful-DOX conjugate **7**. DLS uses a 4-mW He-Ne 633 nm laser at a 173° scattering angle in 2.0-mL 0.2 M sodium phosphate buffer, pH = 6.8.

Cell culture

Monolayers of breast cancer cell lines: MDA-MB-231, T47D, and MCF-7 (purchased from CLS Cell Lines Service) were maintained in RPMI medium supplemented with 10% fetal bovine serum and 1% penicillin/streptomycin. Monolayers of the prostate cancer cell line – PC3 (purchased from American Type Culture Collection – ATCC) – were maintained in the F12K supplemented with 9% fetal bovine serum and antibiotics, as described in ref. [32]. Each cell line was maintained at 37 °C in a humidified atmosphere with 5% CO_2. Ful-DOX and DOX stock solutions in concentration of 1.3 mM and 1 mM, respectively, were prepared in DMSO (for molecular biology use). Control cells were treated with equal amount of pure vehicle (DMSO). The concentration of DMSO in each well was equal to 1%.

Confocal microscopy

MCF-7 cells were incubated with DOX (2 μM) and Ful-DOX conjugate **7** (2 μM) for 48 h at 37 °C. Nuclei were stained using Hoechst 33342 (10 μg/mL). Specimens were imaged using a confocal laser scanning microscope (LeicaSP8X equipped with an incubation chamber for the live analysis) with a 63 × oil immersion lens (Leica, Germany). For DOX, the excitation wavelength was set to 476 nm and emission was detected at 548–650 nm and for Hoechst 33342–405 nm and 449–490 nm, respectively. 3D analyses were made using Leica Application Suite X.

Wst-1 (2-(4-iodophenyl)-3-(4-nitrophenyl) -5-(2,4-disulfophenyl)-2*H* tetrazolium monosodium salt) assay

Cells viability was determined by the WST-1 assay (in which the mitochondrial metabolic activity of cells is measured) as described previously [33]. A total of 4×10^3 cells per well were seeded at a 96-well plate and allowed to attach overnight. Cells were maintained at 37 °C in a humidified atmosphere with 5% CO_2. Next day, the medium was replaced with fresh one supplemented with the tested compounds (in concentration equal to 0.3, 0.5, 1, 2, 3, or 4 μM) or with the pure vehicle (DMSO). Then, the cells were incubated for 48 h. After this time, the WST-1 solution was added and cells were incubated for 3 h. The absorbance values in wells were measured at 440 nm (with the reference wavelength 660 nm) in an EnSpire (PerkinElmer) microplate reader. The viability of control was taken as 100%. Data were obtained from at least

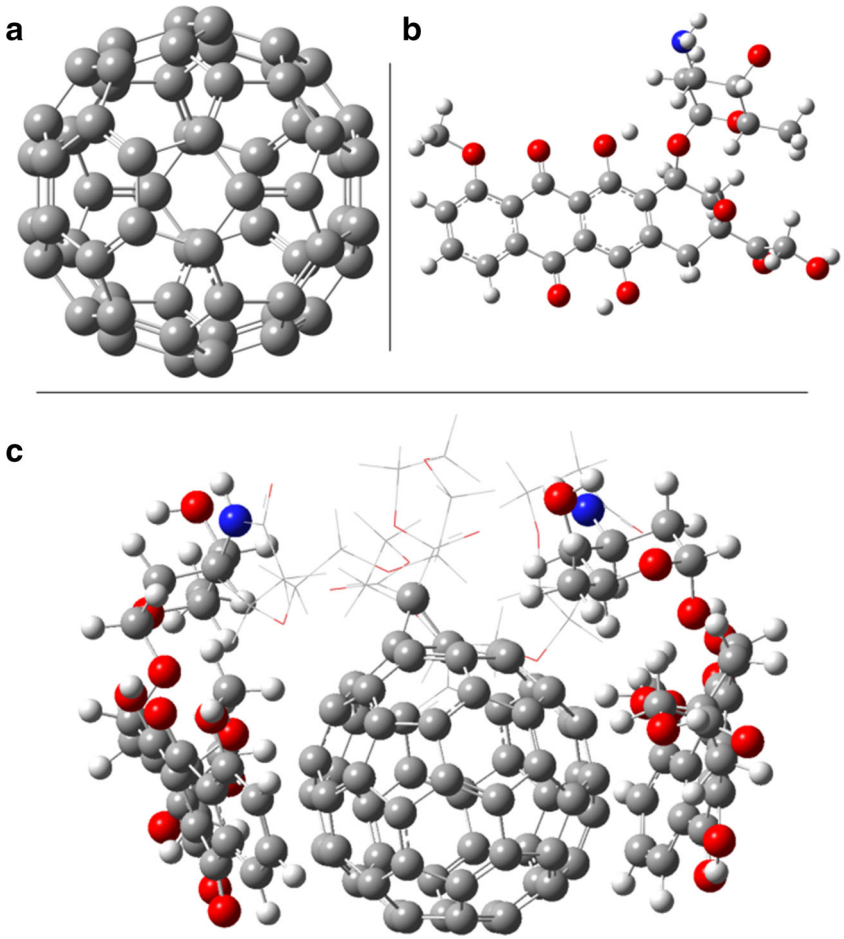

Fig. 2 Ball and stick representation of PM6-D3-optimized structures used for TD-DFT calculations: **a** fullerene, **b** DOX, **c** Ful-DOX conjugate **7** with the linker shown as lines for clarity

two independent experiments, each treatment condition assayed in triplicate.

SRB (sulforhodamine B) assay

SRB assay was performed as described in [34]. Briefly, 4×10^3 cells/well were seeded at 96-well plate. Next day, cells were exposed to indicated concentrations of DOX, Ful-DOX, or pure vehicle (DMSO, control) for 48 h. After this time, medium was removed, and 100 μL/well of 10% trichloroacetic acid was added for 1 h in 4 °C. Afterwards, wells were washed with water, stained with 0.4% sulforhodamine B solution in 1% acetic acid for 15 min, and extensively washed with 1% acetic acid. After addition of 150 μL/well of 10 mM Tris base (pH 10.5), the absorbance was measured at 570 nm with a reference filter of 660 nm in a Victor microplate reader (PerkinElmer). The absorbance of control was taken as 100%. Data were obtained from two independent experiments, each treatment condition assayed in triplicate.

Statistical analysis of Wst-1 and SRB results

The results were analyzed with the use of GraphPad Prism software. The statistical evaluation of treated samples and untreated control was calculated using one-way analysis of variance (ANOVA) followed by Dunnett's multiple comparison test. The data were obtained from at least two independent experiments, and each treatment condition was assayed in triplicate. The differences were considered significant at $\alpha = 0.05$.

Results and discussion

Forming a covalent bond between DOX and fullerene should lead to the lowered cytotoxicity of the drug and its improved pharmacokinetics. Indeed, polymer-drug conjugates may increase tumor-specific download through their enhanced permeability and retention [35]. Moreover, a drug coupled to a polymer may possess increased solubility and resistance to proteolysis, which leads to a better control of pharmacokinetics, including the rate of drug release [36]. Hence, the main idea behind binding of an anticancer drug, which is usually extremely toxic toward healthy cells, to a biocompatible polymer is a safe transportation of the cytostatic to the tumor cells and releasing it only at the target site. However, despite the mentioned above, intuitively understandable idea, there are literature reports, which demonstrate that a doxorubicin conjugate with fullerene is equally toxic as the free DOX. Indeed, in ref. [20], it was demonstrated that the cytotoxicity, measured with the MTT assay using MCF-7 breast cancer cell line, of a fullerene conjugate and DOX was very similar. In order to verify this surprising finding and to reassess the suitability of Ful-DOX conjugates in a possible anticancer therapy, we synthesized a very similar system and studied its physicochemical properties as well as cytotoxicity. Additionally, in order to determine cellular distribution of the studied conjugate, we carried out confocal microscopy analysis of the cells exposed to the conjugate or to the free drug. The results obtained using all methods employed in our study demonstrate that the properties of the conjugate and DOX itself are completely different. Moreover, our findings suggest that binding of DOX to C_{60}-fullerene dramatically lowers its antiproliferative activity. The reason which might explain all discrepancies between our and ref. [20] findings seems to be a considerable contamination of conjugate III [20] with the free DOX and its toxic derivatives.

Conjugate synthesis

There are many synthetic methods for the preparation of fullerene-containing compounds. Fullerene residue exhibits a negative induction effect, which is connected with their electrophilic propensities and possibility to react with different nucleophiles giving fullerene anion intermediates. These include a reaction with C-nucleophiles: (a) Bingel–Hirsch reaction [36] (a formed fullerene anion intermediate is stabilized by an internal addition reaction) and (b) with lithium- [37] or magnesium-organic compounds [38] (a formed fullerene anion intermediate is stabilized by the reaction with various electrophiles). The other example of the nucleophilic reaction with fullerenes is the addition of cyanides followed by the reaction with various nucleophiles [39]. Moreover, fullerenes act as dienophiles, which implicates their ability to undergo cycloaddition. Two types of the aforementioned process are distinguished in the chemical literature: cycloaddition [4+2], i.e., with cyclopentadiene [40], and [3+2], i.e., with diazomethane [41]. Furthermore, fullerenes can be aminated [42], halogenated [43], or hydrogenated [44].

In this study, we obtained a Ful-DOX **7** conjugate using a modified synthetic procedure described by Lu et al. [20]. For the whole synthetic route and chemical structures of all described compounds, see Scheme 1.

In the first step, we obtained a bis(14,14-dimethyl-12-oxo-3,6,9,13-tetraoxapentadecyl) malonate **3** via the reaction of malonyl chloride **1** with *t*-butyl 12-hydroxy-4,7,10-trioxadodecanoate **2** in dry DCM. **2** differs from a corresponding chain shown in ref. [20] by a single $-CH_2-$ group. We were not able to find a commercial substrate that would enable the synthesis of exactly the same structure as described in ref. [19]. Nevertheless, due to size of the system under consideration, two methylene groups (the end-product contains two poly(ethylene glycol) chains each differing by one methylene group from the conjugate described in ref. [20] difference should not influence considerably the physicochemical and/or biological properties of the conjugate.

After 24 h, the reaction was quenched with water, evaporated, and loaded onto the silica gel column. Compound **3** was detected on a TLC plate with the help of iodine to visualize it. Next, a direct functionalization of the malonyl ester derivative **3** was conducted with use of the Bingel–Hirsch reaction. Bis(14,14-dimethyl-12-oxo-3,6,9,13-tetraoxapentadecyl) C_{60}–malonate **4** was obtained by treating the derivative **3** with 1,8-diazabicyclo[5.4.0]undec-7-ene (DBU), carbon tetrabromide (CBr_4), and fullerene-C_{60} in dry toluene. The *t*-butyl ester functions in derivative **4** were subsequently selectively hydrolyzed in the presence of primary esters with trifluoroacetic acid (TFA) [45]. The carboxylic groups present in such obtained 15-C_{60}-14,16-dioxo-4,7,10,13,17,20,23,26-octaoxanonacosane-1,29-dioic acid **5** were then activated with dicyclohexylcarbodiimide (DCC)/*N*-hydroxysuccinimide (NHS) system to give bis(2-(2-(2-(3-((2,5-dioxopyrrolidin-1-yl)oxy)-3-oxopropoxy)ethoxy)ethoxy)ethyl) C_{60}–malonate **6**. At this point, 1,3-dicyclohexylurea (DCU) was obtained as a byproduct and it was impossible to separate it from the compound **6** due to the similarity in their chemical polarity. In the next step, the contaminated active ester **6** was coupled with doxorubicin, freshly obtained via the reaction of doxorubicin hydrochloride with triethylamine in DMF, to give the final Ful-DOX conjugate **7**. At this stage, it was possible to remove DCU from the mixture, because compound **7** is more polar than DCU. The crude product was purified by column chromatography using as an eluent, at first DCM/MeOH 30/1 (to remove DCU from the activation procedure) and then DCM/MeOH 20/1. Initially, we tried to use the eluent suggested by Lu et al. [20] ($CHCl_3$/MeOH 19/1), but it resulted in getting the product **7** contaminated by DCU and other reddish byproducts, presumably derivatives of doxorubicin (for TLC from the last reaction step, see Fig. S7). The structures of compounds **3**–**7** were determined and confirmed by the MALDI-TOF analysis and, in case of compound **3** additionally by the ^{1}H NMR spectrum (see Figs. S1, S2, S3, S4, S5, and S6 in Supplementary Information). In the course of synthesis, it turned out that an electrospray ionization technique is unsuitable to study the structure of the conjugate **7** due to its very weak solubility in polar solvents. The usage of ionization mode employed by the MALDI method resolved the solubility problem. The chemical literature suggests that fullerene-containing compounds tend to fragment, while being irradiated by the laser beam during MALDI analysis [46]. Moreover, in the MALDI ionization source, the doxorubicin moiety can lose the daunosamine and the 1-oxo-2-hydroxyethyl fragment [47]. In consequence, beside a molecular ion peak, fragmentation signals are present on all MALDI spectra included in the supplementary information. The identities of fragments, formed along with their molecular masses, are depicted below particular spectra (see Electronic supplementary material).

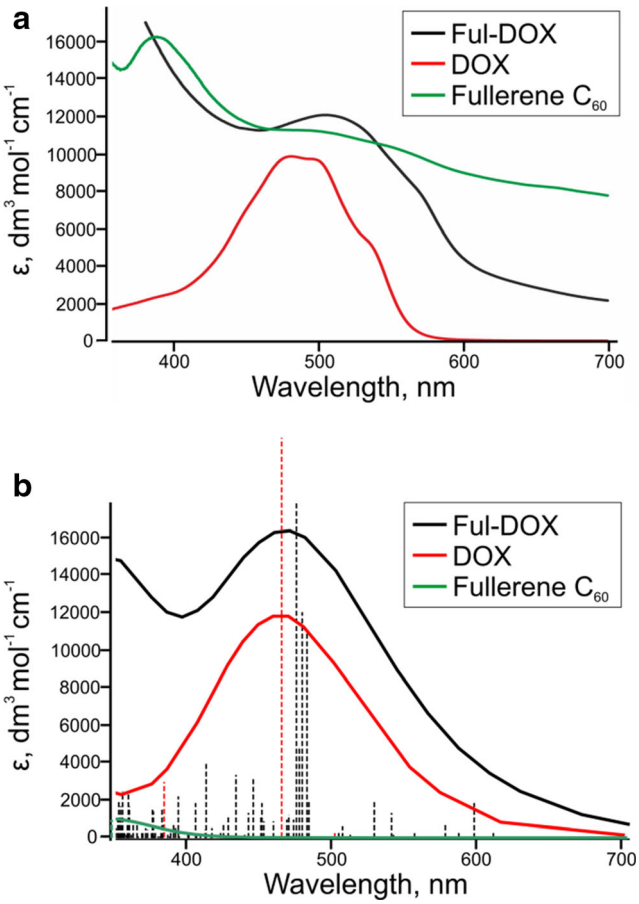

Fig. 3 UV–Vis spectra of DOX, fullerene C_{60}, and Ful-DOX: **a** measured in aqueous DMSO solution; **b** based on the TD-DFT calculations; the oscillator strengths indicated by dotted vertical lines. The scales of oscillator strengths differ for different compounds (cf. the height of vertical lines with the respective oscillator strengths in Table S1)

Physicochemical characteristics

In order to determine the structural features of the new material, aqueous solutions of conjugate **7** were studied by UV–Vis spectrophotometry, spectrofluorimetry, and dynamic light scattering (DLS). All these measurements were carried out using concentrations similar or somewhat larger than those used in biological assays which were primarily a consequence of sensitivity of specific technique. Thus, the UV–Vis spectra were recorded in a 30 μM buffered solution (Fig. 3), fluorescence was measured for Ful-DOX concentrations between 3 and 160 μM and DLS spectrum was obtained for a 15 μM solution of Ful-DOX. Here, it is also worth emphasizing that all the spectra were recorded for Ful-DOX solutions containing, besides buffer, certain amount of DMSO (up to 10%). In all biological tests, Ful-DOX was obtained from a DMSO stock solution and the cells were treated with media containing ca 1% (*v*/*v*) of DMSO.

The absorption spectra of Ful-DOX (29 μM) along with the spectrum of free DOX and C_{60}-fullerene are depicted in Fig.3a. The experimental absorption maximum for DOX

occurs at 481 nm, while for the fullerene, two characteristic peaks at 387 nm and 493 nm are observed. Furthermore, the Ful-DOX spectrum seems to be a superposition of DOX and fullerene features (see Fig.3a). The simulations of experimental spectra based on the TD-DFT calculations are shown in Fig.3b and the most important electronic transitions along with their molecular orbitals are demonstrated in Electronic supplementary material (see Table S1and Fig. S8).

In water, the fullerene forms aggregates and, due to interactions in the solid phase and light scattering, its UV–Vis spectrum is stronger, red-shifted, and broader than the spectra recorded in solvents in which C_{60} forms true solution [48]. The shape of the main long-wavelength absorption peak for Ful-DOX, red-shifted (with regard to DOX) to 506 nm, seems to be a superposition of doxorubicin and fullerene features. However, the maximum extinction coefficient of the conjugate is much smaller than the sum of C_{60} and DOX epsilons (see Fig.3a). Interestingly, the noted above non-additive effect concerning the intensity of electronic transitions was not observed for the UV–Vis spectra published in ref. [20]. Actually, the maximum extinction coefficient of the conjugate (containing two DOX molecules) was ca. 2-fold bigger than that observed for DOX (an additive effect), which suggests lack of interactions between doxorubicin and the fullerene cage for the system studied by Lu et al. [20]. Contrary to their findings, our results indicate strong interactions between doxorubicin and the fullerene cage. Indeed, our quantum chemical calculations suggest that even in water, the conjugate possesses strong tendency to adopt a closed conformation, shown in Fig. 2, in which both DOX molecules interact via stacking with the delocalized π-electrons of the fullerene cage. The geometry optimization that started from the open conformation (both poly(ethylene glycol) chains extended) spontaneously converged to the close one depicted in Fig. 2. Here, it is worth of emphasizing a very good correspondence between the measured and calculated spectra of DOX and Ful-DOX (although the shapes of measured and theoretical spectrum of C_{60} are similar (see Fig. 3), the latter is much weaker). This is a consequence of fullerene aggregation in water which results in strong scattering of incident light [49]). The main wavelength feature of DOX stems from the HOMO ➔ LUMO transition ($\pi\pi^*$ transition; see Table S1). Inspection of molecular orbitals involved in the electronic transitions shows that the HOMO ➔ LUMO transition in DOX corresponds to the one calculated at 480 nm in Ful-DOX (HOMO ➔ LUMO+4; see Table S1). Note, a large difference between the oscillator strengths calculated for DOX (0.29; Table S1) and for the transition involving the same orbitals in Ful-DOX (0.07; Table S1). The visible lowering of oscillator strength is a result of fullerene-DOX interaction. In the remaining transitions (476 and 484 nm) giving rise to the long wavelength feature of Ful-DOX (see Fig. 3b), the occupied orbitals with a considerable contribution from the fullerene are involved. All the above demonstrate strong fullerene-DOX interactions in the conjugate that justifies the non-additive effects observed in the measured absorption spectra.

For the Ful-DOX concentration of up to ca 30 μM, fluorescence intensity increases almost linearly with the amount of conjugate (see the inset to Fig. 4). This suggests that also the number of fluorescing sites increases linearly, which implies, in turn, that the size of aggregates does not change substantially within the discussed concentration range. The presence of Ful-DOX aggregates in the studied aqueous DMSO solution was confirmed by DLS measurements (see Fig. 5). The spectrum presented in Fig. 5 shows that the average hydrodynamic radius for those clusters amount to as much as 838 nm. The maximum intensity of the fluorescence is observed for ca 60 μM and then the fluorescence decreases with concentration. Change in the

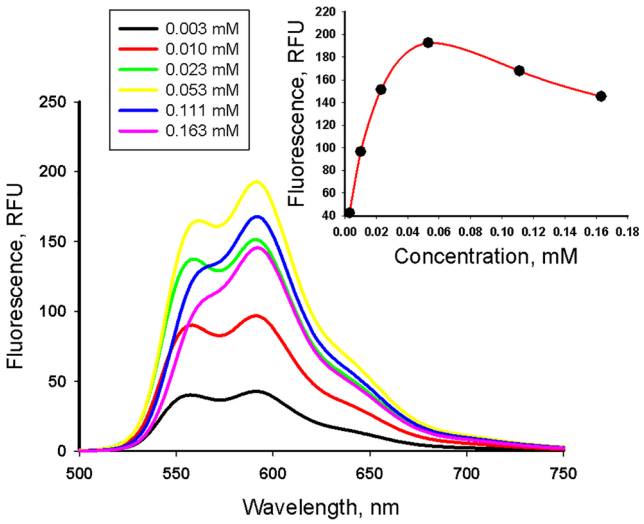

Fig. 4 Concentration effect on the fluorescence spectrum of Ful-DOX conjugate

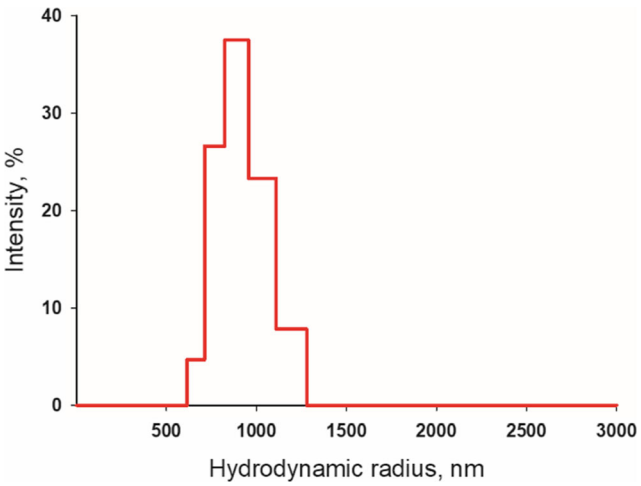

Fig. 5 Dynamic light scattering for an aqueous DMSO solution of Ful-DOX conjugate **7** ($c = 0.015$ mM); average hydrodynamic radius, Z_{avg} = 838 nm

shape of spectrum with increasing amount of Ful-DOX (see Fig. 4) suggests a trivial mechanism of quenching (reabsorption) [49]. Actually, the short-wavelength band of fluorescence gradually disappears for more concentrated solutions, which suggests reabsorption. Indeed, there is a strong overlap between the absorption and emission spectra of Ful-DOX in the range of 550–600 nm (cf. Figs. 3 and 4).

Impact of Ful-DOX on the viability of cancer cells

The main purpose of our study was to elucidate whether the binding of DOX to a non- or low-toxic carrier should alleviate the toxicity of doxorubicin. Actually, only then such construct might be used as a safe platform that enables toxic chemotherapeutics to be transported and released in the target cell. We compared viability of cells treated for 48 h with doxorubicin or Ful-DOX conjugate. To exclude that results might be cell line specific, we used cancer cells derived from different organs, namely breast (MCF-7, T47D, and MDA MB 231 cell lines) and prostate (PC3 cell line). Breast cancer cells represent different molecular subtypes of this malignancy: MCF-7 and T47D cells are of luminal type characterized by the presence of estrogen receptor (ER) and progesterone receptor (PR) while MDA MB 231 cells are so called triple negative as they are negative for ER, PR, and human epithelial receptor 2 (HER2) and represent the most aggressive and one of the worst prognosis breast cancer subtype. Moreover, two types of viability assays have been used: SRB measuring total proteins in the cells and WST-1 which, similarly as MTT, indicates metabolically active cells.

As shown in Figs. 6 and 7, Ful-DOX in the studied range of concentrations demonstrates no or very low effect on viability of all tested cell lines, whereas free DOX reduces viability in a dose-dependent manner with IC50 ca 1 (MDA MB 231 and

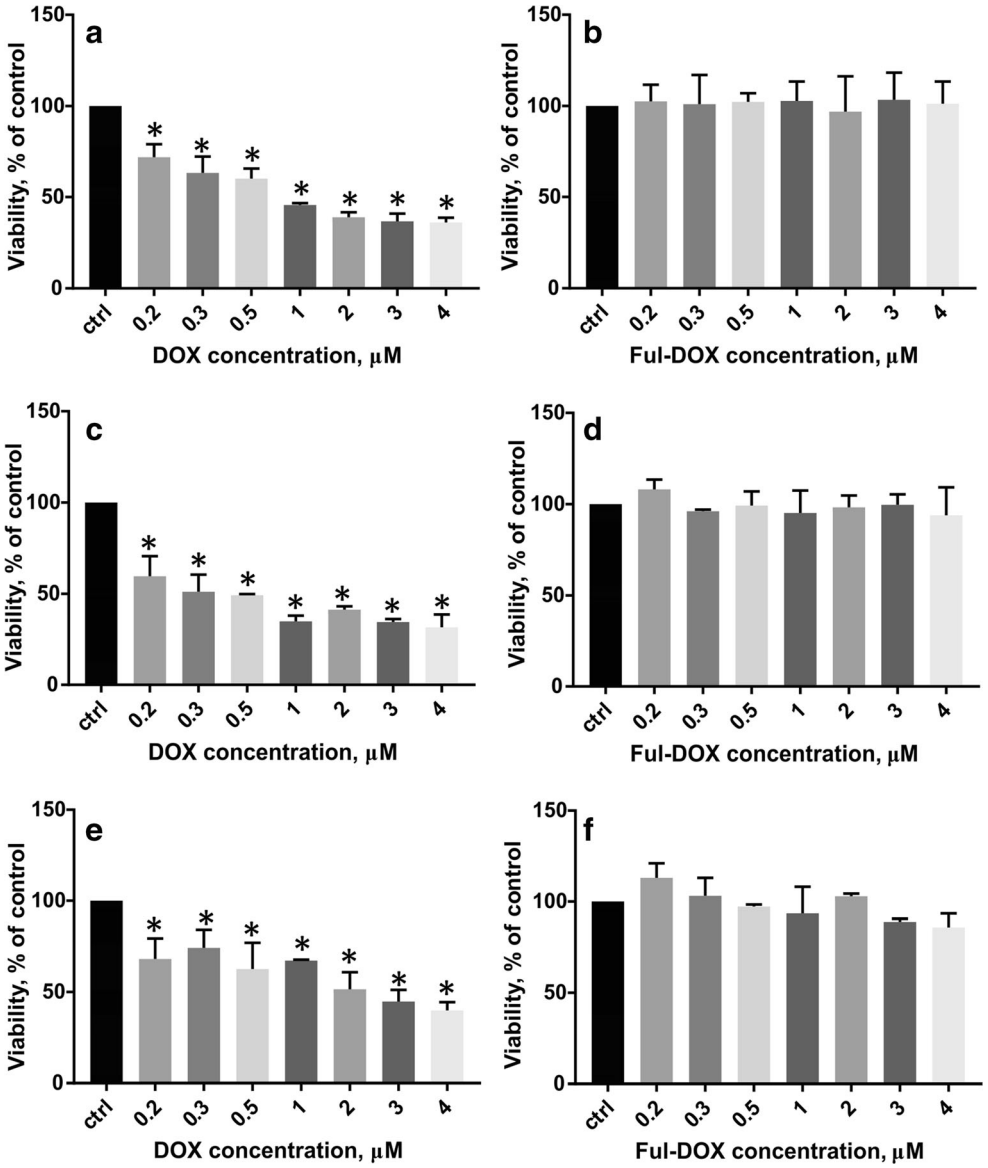

Fig. 6 The viability of MDA-MB-231 (**a**, **b**), MCF-7 (**c**, **d**), and T47D (**e**, **f**) cells after 48-h treatment with doxorubicin and Ful-DOX conjugate **7** in a range of concentrations from 0 (control; ctrl) to 4 μM assessed by the SRB assay. Results are shown as mean ± SD of two independent experiments performed in triplicate. *Statistically significant difference between the treated and control (untreated sample) at $\alpha = 0.05$

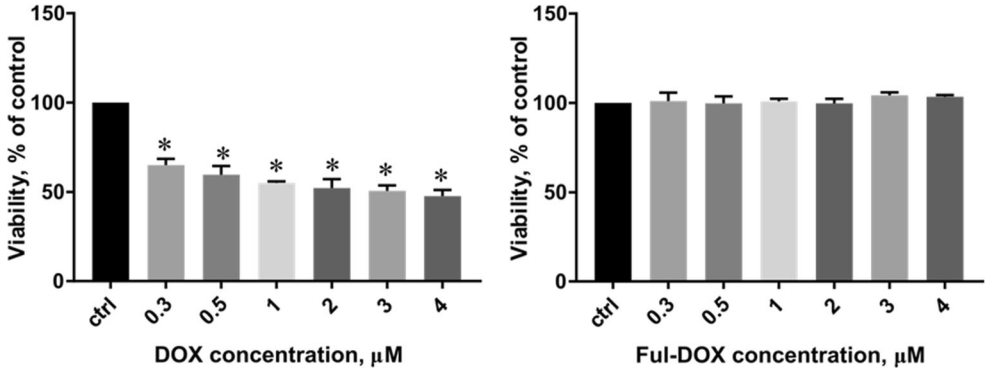

Fig. 7 The viability of PC3 cells after 48 h of treatment with doxorubicin and Ful-DOX conjugate **7** in a range of concentrations from 0 (control; ctrl) to 4 μM determined by the WST-1 assay. Results are shown as mean ± SD of two independent experiments performed in triplicate. *Statistically significant difference is present between treated samples compared with control (untreated sample) at $\alpha = 0.05$

MCF-7 cells) or 2 μM (T47D and PC-3 cells). It is worth noting that results of the WST-1 assay, which is much simpler than the SRB one (see the Methods section), show marginal standard deviations (see Fig. 7). Presented results remain in apparent discrepancy with those reported by Lu et al. [20]. They observed no difference between Dox and Ful-DOX activity towards MCF-7 cells as assessed by MTT assay. Moreover, Ful-DOX at the concentration of 10 μg/mL, which roughly corresponds to our 4 μM, reduced viability of cells by about 40% compared with untreated controls after 24-h exposition. It contrasts with our results which indicate lack of toxicity of the conjugate, despite the fact that in our experiments, the cells were treated for longer time (48 h).

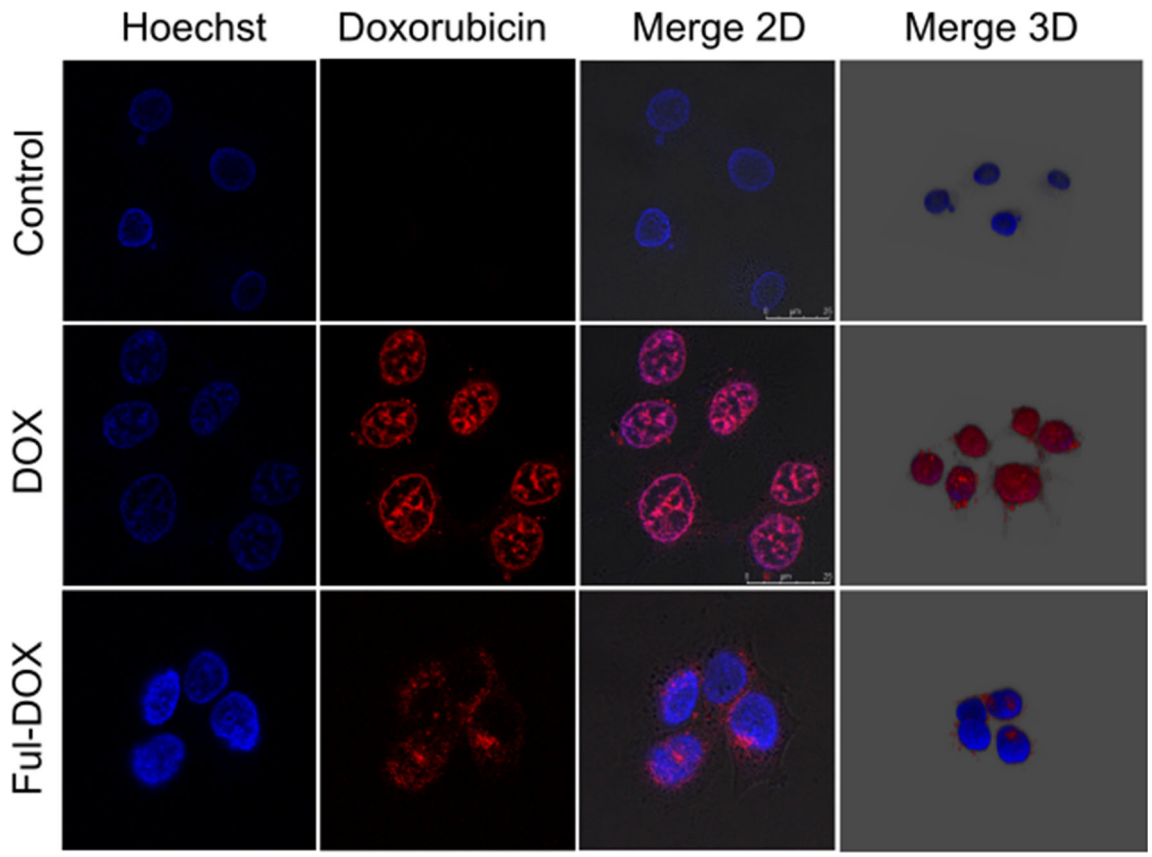

Fig. 8 Images from confocal microscope of MCF-7 cells treated with 2 μM DOX and 2 μM Ful-DOX conjugate **7**. Nuclei are stained blue using Hoechst 33342, red color emitted by doxorubicin moieties, 2D and 3D merged images including the Hoechst dye and DOX or Ful-DOX **7** emission show cellular localization. The MCF-7 cells were incubated at with tested agents for 48 h. Scale bars are 25 μm

Confocal microscopy

In order to verify our conclusions, we also carried out measurements concerning the distribution of free DOX and the conjugate in cells. Since DOX is a good fluorophore, we decided to employ confocal microscopy. Figure 8 gathers several confocal 2D and 3D images showing cellular distribution of DOX or full-DOX.

Cell nuclei are depicted by blue spots as they were stained with Hoechst 33342. On the other hand, DOX emits a red fluorescence. As indicated by the middle panel of Fig. 8, free DOX penetrates into the nuclei (DOX/Merge 2D, Fig. 8) as well as adsorbs on nuclear membrane (DOX/Merge 3D, Fig. 8). The behavior of Ful-DOX is quite different. It does not penetrate into the nuclei but accumulates on their membranes (Ful-DOX/Merge 2D and Ful-DOX/Merge 3D, Fig. 8). Taking into account the physicochemical properties of Ful-DOX, i.e., strong interactions between DOX and fullerene cage, chemically stable linker, as well as the size of hydrodynamic radius of nanoparticles which Ful-DOX forms in the buffered aqueous solution, one can expect that an efficient nucleus penetration, which seems to be indispensable for the DOX cytotoxic action, is reduced or abolished in case of the conjugate.

Conclusions

In this study, we synthesized a fullerene-DOX conjugate, measured its physicochemical characteristics, and determined its toxicity and the cellular distribution with the viability assays and confocal microscopy, respectively. The physicochemical characteristics indicate strong interactions between the fullerene cage and doxorubicin in the Ful-DOX as well as the formation of voluminous clusters of the conjugate under the conditions employed in the cellular studies. These explain the observed lack of cytotoxicity. Indeed, to be toxic, doxorubicin has to penetrate into the nucleus in order to directly interact with DNA or protein machinery dedicated to DNA processing. Being covalently bound to the fullerene-poly(ethylene glycol) moiety and additionally forming sizable clusters, DOX possibilities to interact with DNA are very limited. Moreover, a nuclear membrane does not support endocytosis and its pores are able to accommodate particles up to only about 25 nm diameter [50], while the synthesized Ful-DOX conjugate forms clusters with an average hydrodynamic radius of ca. 800 nm.

In summary, our study demonstrates that the studied conjugate has a potential to become a universal platform for safe transportation of toxic drugs into tumor cells. A quest for molecular modifications and implementation of DOX conjugates specifically releasing the drug is currently under way in our laboratories.

Funding information This work was supported by the Polish Ministry of Science and Higher Education under Grants Nos. DS 530-8227-D494-18 (J. R.) and DS 530-M045-D674-18 (J. P.). The calculations were performed in the Wroclaw Center for Networking and Supercomputing, grant No. 209.

Compliance with ethical standards

Conflict of interest The authors declare that they have no conflicts of interest.

References

1. Abushouk AI, Ismail A, Salem AMA, Afifi AM, Abdel-Daim MM (2017) Cardio protective mechanisms of phytochemicals against doxorubicin-induced cardiotoxicity. Biomed Pharmacother 90: 935–946
2. Mobaraki M, Faraji A, Zare M, Dolati P, Ataei M, Dehghan Manshadi HR (2017) Molecular mechanisms of cardiotoxicity: a review on the major side-effect of doxorubicin. Indian J Pharm Sci 79:335–344
3. Gewirtz DA (1999) A critical evaluation of the mechanisms of action proposed for the antitumor effects of the anthracycline antibiotics adriamycin and daunorubicin. Biochem Pharmacol 57:727–741
4. Box V (2007) The intercalation of DNA double helices with doxorubicin and nagalomycin. J Mol Graph Mod 26:14–19
5. Chatterjee K, Zhang J, Honbo N, Karliner JS (2010) Doxorubicin cardiomyopathy. Cardiology 115:155–162
6. Carvalho C, Santos RX, Cardoso S, Correia S, Oliveira PJ, Santos MS, Moreira PI (2009) Doxorubicin: The good, the bad and the ugly effect. Curr Med Chem 16:3267–3285
7. Takemura G, Fujiwara F (2007) Doxorubicin-induced cardiomyopathy: from the cardiotoxic mechanisms to management. Prog Cardiovasc Dis 49:330–352
8. Swain S, Whaley F, Ewer M (2003) Congestive heart failure in patients treated with doxorubicin. Cancer 97:2869–2879
9. von Hoff DD, Layard MW, Basa P, Davis HL, von Hoff AL, Rozencweig M, Muggia FM (1979) Risk factors for doxorubicin-induced congestive heart failure. Ann Intern Med 91:710–717
10. Cirillo R, Sacco G, Venturella S, Brightwell J, Giachetti A, Manzini S (2000) comparison of doxorubicin – and MEN 10755 – induced long-term progressive cardiotoxicity in the rat. J Cardiovasc Pharmacol 35:100–108
11. Wallace KB (2007) Adriamycin-induced interference with cardiac mitochondrial calcium homeostasis. Cardiovasc Toxicol 7:101–107
12. Nousiainen T, Jantunen E, Vanninen E, Remes J, Vuolteenaho O, Hartikainen J (1999) Natriuretic peptides as markers of cardiotoxicity during doxorubicin treatment for non-Hodgkin's Lymphoma. Eur J Haematol 62:135–141
13. Chen B, Peng X, Pentassuglia L, Lim CC, Sawyer DB (2007) Molecular and cellular mechanisms of anthracycline cardiotoxicity. Cardiovasc Toxicol 7:114–121

14. Anilkumar P, Lu F, Cao L, Luo PG, Liu J-H, Sahu S, Tackett II KN, Wang Y, Sun Y-P (2011) Fullerenes for Applications in Biology and Medicine. Curr Med Chem 18:2045–2059
15. Zhang X, Cong H, Yu B, Chen Q (2019) Recent advances of water-soluble fullerene derivatives in biomedical applications. Mini-Rev Org Chem 16:92–99
16. Kepinska M, Kizek R, Milnerowicz H (2018) Fullerene as a doxorubicin nanotransporter for targeted breast cancer therapy: Capillary electrophoresis analysis. Electrophoresis 39:2370–2379
17. Chaudhuri P, Paraskar A, Soni S, Mashelkar RA, Sengupta S (2009) Fullerenol-cytotoxic conjugates for cancer chemotherapy. ACS Nano 3:2505–2514
18. Panchuk R, Prylutska S, Skorokhyd N, Lehka L, Skivka L, Hurmach V, Evstigneev M, Piosik J, Berger W, Prylutskyy Y, Scharff P, Stoika R, Vari S. Enhancement of anticancer action of traditional (doxorubicin and cisplatin) and experimental (landomycin A) drugs by their delivery in vivo with novel C60-fullerene-based nanocarrier possessing innate ROS-modulating activity, 11th Annual TechConnect World Innovation Conference and Expo, Washington, United States, 14.05–17.05.17
19. Zakharian TY, Seryshev A, Sitharaman B, Gilbert BE, Knight V, Wilson LJ (2005) A fullerene-paclitaxel chemotherapeutic: Synthesis, characterization, and study of biological activity in tissue culture. J Am Chem Soc 127:12508–12,509
20. Shi J, Wang B, Wang L, Lu T, Fu Y, Zhang H, Zhang Z (2016) Fullerene (C_{60})-based tumor-targeting nanoparticles with "off-on" state for enhanced treatment of cancer. J Contr Release 235:245–258
21. Lu F, Haque SA, Yang S-T, Luo PG, Gu L, Kitaygorodskiy A, Li H, Lacher S, Sun Y-P (2009) Aqueous compatible fullerene–doxorubicine conjugates. J Phys Chem C 113:17768–17,773
22. Liu J-H, Cao L, Luo PG, Yang S-T, Lu F, Wang H, Meziani MJ, Haque AS, Liu Y, Lacher S, Sun Y-P (2010) Fullerene-conjugated doxorubicin in cells. ACS Appl Mater Inter 2:1384–1389
23. Stewart JJP (2007) Optimization of parameters for semiempirical methods. V. Modification of NDDO approximations and application to 70 elements. J Mol Model 13:1173–1213
24. Grimme S, Antony J, Ehrlich S, Krieg H (2010) A consistent and accurate ab initio parametrization of density functional dispersion correction (DFT-D) for the 94 elements H-Pu. J Chem Phys 132: 154104
25. Runge E, Gross EK (1984) Density-functional theory for time-dependent systems, Phys Rev. Lett 52:997–1000
26. Weigend F, Ahlrichs R (2005) Balanced basis sets of split valence, triple zeta valence and quadruple zeta valence quality for H to Rn: Design and assessment of accuracy. Phys Chem Chem Phys 7: 3297–3305
27. Weigend F (2006) Accurate coulomb-fitting basis sets for H to Rn. Phys Chem Chem Phys 8:1057–1065
28. Cossi M, Barone V, Cammi R, Tomasi J (1996) Ab initio study of solvated molecules: a new implementation of the polarizable continuum model. Chem Phys Lett 255:327–335
29. Miertuš S, Scrocco E, Tomasi J (1981) Electrostatic interaction of a solute with a continuum. A direct utilization of ab initio molecular potentials for the prevision of solvent effects. J Chem Phys 55:117–129
30. Kariminasab M, Tajbakhsh M, Ganji MD, Alinezhad H (2017) A theoretical investigation of the structural, electronic and UV–vis absorption spectra of fullerene derivatives based on PC61B-NHCS compound. Mater Chem Phys 199:597–608
31. Frisch MJ, Trucks GW, Schlegel HB, Scuseria GE, Robb MA, Cheeseman JR, Scalmani G, Barone V, Mennucci B, Petersson GA, et al. (2009) Gaussian 09 (Rev. D.01), Gaussian, Inc., Wallingford, CT
32. Hać A, Domachowska A, Narajczyk M, Cyske K, Pawlik A, Herman-Antosiewicz A (2015) S6K1 controls autophagosome maturation in autophagy induced by sulforaphane or serum deprivation. Eur J Cell Biol 94:470–481
33. Tominaga H, Ishiyama M, Ohseto F, Sasamoto K, Hamamoto T, Suzuki K, Watanabe M (1999) A water-soluble tetrazolium salt useful for colorimetric cell viability assay. Anal Comm 36:47–50
34. Pawlik A, Wała M, Hać A, Felczykowska A, Herman-Antosiewicz A (2017) Sulforaphene, an isothiocyanate present in radish plants, inhibits proliferation of human breast cancer cells. Phytomedicine 29:1–10
35. Veronese FM, Schiavon O, Pasut G, Mendichi R, Andersson L, Tsirk A, Ford J, Wu G, Kneller S, Davies J, Duncan R (2005) PEG-doxorubicin conjugates: influence of polymer structure on drug release, in vitro cytotoxicity, biodistribution, and antitumor activity. Bioconjugate Chem 16:775–784
36. Nakamura Y, Suzuki M, Imai Y, Nishimura J (2004) Synthesis of [60] fullerene adducts bearing carbazole moieties by Bingel reaction and their properties. Org Lett 6:2797–2799
37. Hirsch A, Brettreich M (2005) Fullerenes: chemistry and reactions, pp. 73–99, Wiley-VCH Verlag GmbH & Co. KGaA
38. Yan W, Seifermann SM, Pierrat P, Bräse S (2015) Synthesis of highly functionalized C_{60} fullerene derivatives and their applications in material and life sciences. Org Biomol Chem 13:25–54
39. Komatsu K, Wang G-W, Murata Y, Tanaka T, Fujiwara K (1998) Mechanochemical synthesis and characterization of the fullerene dimer C_{120}. J Org Chem 63:9358–9366
40. Schlueter JA, Seaman JM, Taha S, Cohen H, Lykke KR, Wang HH, Williams JM (1993) Synthesis, purification, and characterization of the 1: 1 addition product of C_{60} and anthracene. J. Chem Soc Chem Commun 11:972–974
41. Prato M, Li QC, Wudl F, Lucchini V (1993) Addition of azides to fullerene C_{60}: synthesis of azafulleroids. J Am Chem Soc 115: 1148–1150
42. Hu X, Jiang Z, Jia Z, Huang S, Yang X, Li Y, Gan L, Zhang S, Zhu D (2007) Amination of [60]fullerene by ammonia and by primary and secondary aliphatic amines – preparation of amino[60]fullerene peroxides. Chem Eur J 13:1129–1141
43. Olah GA, Bucsi I, Lambert C, Aniszfeld R, Trivedi NJ, Sensharma DK, Prakash GKS (1991) Chlorination and bromination of fullerenes. Nucleophilic methoxylation of polychlorofullerenes and their aluminum trichloride catalyzed friedel–crafts reaction with aromatics to polyarylfullerenes. J Am Chem Soc 113:9385–9387
44. Monakov YB, Zaikov GE (2006) Molecular and high molecular chemistry: theory and practice. Science publishers, Nova, pp 1–47
45. Greene TW, Wuts PGM (1999) Protective groups in organic synthesis, vol 65–67. Wiley, New York, pp 404–408
46. Trimpin S, Keune S, Räder HJ, Müllen K (2006) Solvent-free Maldi-MS: developmental improvements in the reliability and the potential of maldi in the analysis of synthetic polymers and giant organic molecules. J Am Soc Mass Spectrom 17:667–671
47. Di Francesco R, Griggs JJ, Donnelly J, Di Cenzo R (2007) Simultaneous analysis of cyclophosphamide, doxorubicin and doxorubicinol by liquid chromatography coupled to tandem mass spectrometry. J Chromatogr B 852:545–553
48. Chang X, Vikesland PJ (2011) UV-vis Spectroscopic properties of nC_{60} produced via extended mixing. Environ Sci Technol 45:9967–9974
49. Bowen EJ (1968) Luminescence in chemistry. D. Van Nostrand Reinhold Ltd., Princeton, p 154
50. Stewart M (1992) Nuclear pore structure and function. Semin Cell Biol 3:267–277